J Mater Sci: Mater Med (2011) 22:2197–2206
DOI 10.1007/s10856-011-4417-1

Magnetic bioactive glass ceramic in the system $CaO–P_2O_5–SiO_2–MgO–CaF_2–MnO_2–Fe_2O_3$ for hyperthermia treatment of bone tumor

Guangda Li · Shuying Feng · Dali Zhou

Received: 2 March 2011 / Accepted: 6 August 2011 / Published online: 26 August 2011

Abstract Magnetic bioactive glass ceramic (MG) in the system $CaO–SiO_2–P_2O_5–MgO–CaF_2–MnO_2–Fe_2O_3$ for hyperthermia treatment of bone tumor was synthesized. The phase composition was investigated by XRD. The magnetic property was measured by VSM. The in vitro bioactivity was investigated by simulated body fluid (SBF) soaking experiment. Cell growth on the surface of the material was evaluated by co-culturing osteoblast-like ROS17/2.8 cells with materials for 7 days. The results showed that MG contained $CaSiO_3$ and $Ca_5(PO_4)_3F$ as the main phases, and $MnFe_2O_4$ and Fe_3O_4 as the magnetic phases. Under a magnetic field of 10,000 Oe, the saturation magnetization and coercive force of MG were 6.4 emu/g and 198 Oe, respectively. After soaking in SBF for 14 days, hydroxyapatite containing CO_3^{2-} was observed on the surface of MG. The experiment of co-culturing cells with material showed that cells could successfully attach and well proliferate on MG.

G. Li · S. Feng
College of Medical Technology and Engineering, Henan University of Science and Technology, Luo Yang 471003, Henan, People's Republic of China

G. Li
e-mail: scdxlgd@yahoo.cn

G. Li · D. Zhou (✉)
College of Material Science and Engineering, Sichuan University, Chengdu 610068, Sichuan, People's Republic of China
e-mail: zdl@scu.edu.cn

1 Introduction

Since Hench et al. first discovered Bioglass in 1970s, large number of studies have focused on bioactive glasses and glass ceramics [1]. Recently, development of glass–ceramics with good bioactivity and magnetic property has attracted much attention [2–6].

Magnetic bioactive glass ceramics are specially designed to restore bone tissue after tumor extirpation. On the one hand, this kind of glass ceramic is bioactive, when soaked in SBF or implanted in the living body, a biologically active apatite layer which can bond to the weakened tumorous bone forms on the surface [3, 4]. On the other hand, this kind of glass–ceramic is magnetic and has the ability to act as thermoseeds for cancer treatment using hyperthermia [7]. Under an alternative magnetic field, this material is able to generate heat due to hysteresis loss. When this material is placed in the region of the tumor and is subjected to an alternating magnetic field, the heat from thermoseeds raises the temperature of the surrounding. Since above 43°C the cancerous cells are the first to die when a heat treatment is applied [4, 7],when the temperature rise to 42–45°C, the cancerous cells perish while the healthy ones survive [6]. Moreover, after the removal of a tumor,the malignant cells can remain around the tumor site, leading to tumor recurrence, with fatal consequences [8]. Magnetic bioactive glass ceramic implant can undergo the re-heat process when necessary, and kill the malignant cells to prevent the tumor recurrence. Additionally, the harmful leaching of metal ions into human body fluid by these materials can be avoided due to the encapsulation of each ferromagnetic particle by the glass matrix [9].

Since magnetic bioactive glass ceramic is an excellent alternative to restore bone defects that occur after tumor extirpation, magnetic bioactive glass–ceramics in different

systems have been synthesized. Luderer et al. initially reported a non-bioactive glass–ceramic system with lithium ferrite ($LiFe_5O_8$) and magnetite (Fe_3O_4) in an Al_2O_3–SiO_2–P_2O_5 glassy matrix [10]. Then Ebisawa et al. prepared another non-bioactive one with Fe_3O_4 in a matrix of $CaO{\cdot}SiO_2$-based glass and wollastonite (CaO–SiO_2) [11]. In their later study, glass–ceramics with Na_2O or B_2O_3 added in combination with P_2O_5 was found to show bioactivity [3]. More magnetic glass–ceramics with bioactivity were reported since then. Bretcanu et al. prepared a bioactive glass–ceramic in the system SiO_2–Na_2O–CaO–P_2O_5–FeO–Fe_2O_3 [12]. Shah et al. synthesized the system ZnO–Fe_2O_3–CaO–SiO_2–P_2O_5–Na_2O containing Zn ferrite [13, 14]. Chi-Shiung et al. reported the system Li_2O–MnO_2–CaO–P_2O_5–SiO_2–Fe_2O_3 containing (Li, Mn) ferrite phase [15]. Tzu-Wei et al. prepared a degradable one in the Na_2O–CaO–P_2O_5–SiO_2–Fe_2O_3 system [16].

In present study, we planed to synthesize magnetic bioactive glass ceramic by doping MnO_2 and Fe_2O_3 to the CaO–SiO_2–P_2O_5–MgO–CaF_2 matrix. The apatite–wollastonite containing glass ceramic in the system CaO–SiO_2–P_2O_5–MgO–CaF_2 was first prepared by Kokubo in 1980s. This glass–ceramic has high bioactivity, good biocompatibility and mechanical property, and has been used clinically and studied widely [17]. Recently, Sharma et al. reported a magnetic glass ceramic in this system with good properties [18]. In our previous studies, magnetic bioactive glass ceramics with Mg ferrite and Mn–Zn ferrite in this matrix were synthesized, and good magnetic property and bioactivity was observed [19, 20]. Thus the bioactive CaO–SiO_2–P_2O_5–MgO–CaF_2 system was chosen in present study.

The motivation for the addition of Mn is due to its good biological property and magnetic property. This biologically important metal manganese is an essential key cofactor for metalloenzymes (oxidases and dehydrogenases), DNA polymerases and kinases [21]. The deficiency of manganese may result in the delayed osteogenesis process due to lower activity of osteoblasts. This may lead to bone deformation, growth inhibition, worse movement co-ordination, and even to bone resorption [22]. Moreover, Mn divalent cation is known to linked to the activation of integrins, a family of receptors which mediate cellular interaction with extracellular matrix and cell surface ligands. In the presence of Mn^{2+} ions the ligand affinity of integrin increases and cell adhesion is promoted [23]. Biological tests demonstrated that the Mn-doped HA coatings on etched Ti substrates can favour osteoblasts proliferation, activation of their metabolism and differentiation [24]. Furthermore, Sima et al. proved in their investigations that manganese has a beneficial effect on viability and spread of cells cultured on thin Mn-β-TCP film coatings on titanium [25]. Therefore, divalent Mn cation supplementation of biomaterials could be a promising approach to improve the ingrowth and the integration of implants.

In addition, Mn is an important magnetic element. Mn ferrite has good magnetic properties, and is widely used in electrical equipment and for electronic applications [26, 27]. Recently, much effort has gone into the application of Mn ferrite in cases of hyperthermia [27, 28]. Though Mn ferrite has already been introduced to magnetic bioactive glass–ceramics in previous study, the cell behaviour on the materials was not reported [15]. In present study, oxides MnO_2 and Fe_2O_3 were doped to the bioactive matrix, and magnetic bioactive glass–ceramic in the system CaO–SiO_2–P_2O_5–MgO–CaF_2–MnO_2–Fe_2O_3 was synthesized. Specially, the cell affinity of the material was tested.

2 Experimental

2.1 Preparation of materials

Firstly, Mn ferrite precursor was prepared. Analytical reagent MnO_2 and Fe_2O_3 were weighted in the molar ration of 1/1, and mixed with an agate mortar. The mixture was heated at 980°C for 1.5 h in air atmosphere in a furnace (heating rate 2°C/min). Then the obtained precursor was ground and 300-mesh sieved. The sieved precursor was heated at 1,200°C for 2 h, and Mn ferrite was obtained as contrast.

Secondly, the precursor of wollastonite–fluorapatite-containing bioactive glass–ceramic (BG) was prepared. And BG was in the nominal composition of 45CaO–$33SiO_2$–$16P_2O_5$–4.5MgO–$0.5CaF_2$ (% weight). BG gel was obtained through sol–gel method as Ming [29]. The gel was dried in an oven at 100°C for 24 h. Precursor was obtained by calcining the dried gel at 800°C for 1 h and at 1,150°C for 2 h (heating rate 2°C/min from 20 to 800°C, 5°C/min from 800 to 1,150°C). Then the precursor was ground and 200-mesh sieved.

To synthesize magnetic bioactive glass–ceramics (MG), the BG precursor and the ferrite precursor were mixed in a weight ratio of 10/1, and blended with 2 wt% polyvinyl alcohol. The mixture was dry-pressed into pellets (ø10 mm × 3 mm and ø10 mm × 2 mm) in a steel die at 16 Mpa. The compacts were sintered at l,200°C for 2 h in air atmosphere (heating rate 2°C/min), then quenched in air. BG was synthesized as contrast. The BG precursor was pressed and sintered in the same way as MG.

In order to maintain the homogeneity of the material, the as obtained samples were polished lightly with SiC abrasive paper (P500). Then samples were washed successively in deionized water and ethanol using ultrasound cleaner. Subsequently, the samples were dried at 110°C for 1 h.

2.2 Sample characterization

2.2.1 *Phase composition and magnetic property*

The dried samples were crushed and ground into powders. The phase composition of the samples was detected by X-Ray diffractometer (XRD, Philips X'Pert Pro MDP). Magnetic properties were measured by a vibrating sample magnetometer (VSM, Lake shore 7410) at room temperature. BG was mixed with Mn ferrite (heated at 1200°C for 2 h) in the weight ratio of 10/1, and the phase composition and magnetic property of the mixture were measured as contrast. The magnetic property of MG soaked in simulated body fluid (SBF) for 30 days were also detected. The soaking process was the same as the in vitro bioactivity test.

2.2.2 *In vitro bioactivity*

The dried samples were soaked in SBF at 37°C under continuous shaking for various times [30], and a constant solid mass/liquid volume (0.25 g/50 ml) ratio was maintained. The pH-values in SBF were detected by a pH meter. The Ca^{2+} concentrations in SBF were measured by atomic absorption spectrometry analyses (AAS, 180-80, HITACH). The tests were repeated five times. Statistical analyses were performed using Origin8.0 (Origin Lab Corporation, Northampton, MA, USA) at a significance level of $P < 0.05$.

After intervals of 7 and 14 days, the samples were removed from SBF, carefully rinsed twice with deionized water and dried at 110°C for 1 h. The surface morphology of the sample was observed by scanning electron microscope (SEM, JSM-5900LV, HITACH). The deposits grown on the samples were carefully detached. Then the detached deposits were detected by FT-IR (SPECTRUM 2000, Perkin-Elmer Co.,) and XRD.

2.2.3 *Cell culturing*

Osteoblast-like ROS17/2.8 cells were maintained at 37°C under 5% CO_2 and 95% air in a humidified incubator. The cells were grown in DMEM medium supplemented with 10% (v/v) fetal bovine serum, 500 UI/ml of penicillin and 0.1 mg/ml of streptomycin. The medium was changed for fresh medium every 2 days.

The washed MG samples were sterilized by dry heat at 180°C for 2 h. The sterilized materials were put into 24-well plates and immersed in 5 ml of culture medium [31]. The culture medium was removed 72 h later, and ROS17/2.8 cells at the density of 2×10^4 cm^{-2} were seeded directly on the surface of MG in each culture well. On day 3 and 7, cell morphology on the material was evaluated by observing the cells using SEM. At the end of the incubation time, the specimens were washed four times with PBS. Subsequently, cell fixation was carried out in 2 wt% glutaraldehyde for 4 h at room temperature. Then samples were dehydrated in ethanol with ascending gradient concentration from 35 to 100%, and dried in the critical point [32]. After Au coating, SEM was used to detect attachment and morphology of cells on the material.

3 Results and discussion

3.1 Phases composition

The XRD patterns of MG, BG and the mixture of BG and ferrite in the weight ratio of 10/1 are shown in Fig. 1. The patterns demonstrate the presence of a mixture of crystalline phases for all the materials. BG contains three prominent crystalline phases: wollastonite ($CaSiO_3$) [PDF # 84-0654], akermanite ($Ca_2MgSi_2O_7$) [PDF #77-1149] and fluorapatite ($Ca_5(PO_4)_3F$) [PDF #71-0881]. The major phases of the BG and ferrite mixture not only include these three phases from the glass ceramic but also iwakiite ($MnFe_2O_4$)[PDF # 38-0430] from the ferrite. And magnetite (Fe_3O_4) [PDF # 16-0629] is observed to be the minor phase in the mixture. The composition of MG is even more complicated than BG and the mixture. The main phases of MG are wollastonite ($CaSiO_3$) and fluorapatite ($Ca_5(PO_4)_3F$). Simultaneously iwakiite $MnFe_2O_4$ [PDF # 38-0430], magnetite (Fe_3O_4) [PDF # 16-0629], pigonite ($(Fe,Mg,Ca)SiO_3$) [PDF # 13-0421] and johannsenite ($CaMnSi_2O_6$) [PDF # 38-0413] are detected due to the doping of oxides. When compared the patterns of MG with that of the mixture, remarkable differences are observed. First of all, much more $MnFe_2O_4$ was observed in the mixture than in MG. In order to obtain $MnFe_2O_4$ in high quality, quenching method was used for both materials [33]. Nevertheless only a little $MnFe_2O_4$ was

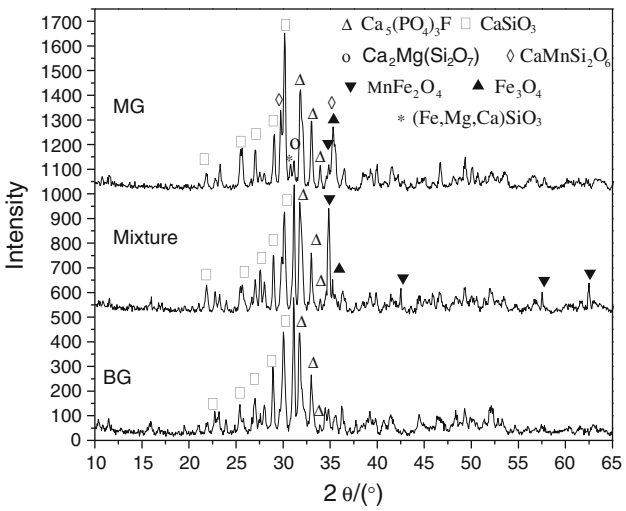

Fig. 1 XRD patterns of BG, MG and the BG and ferrite mixture

observed in MG. This phenomena could be explained by the fact that the doping oxides reacted with the BG matrix during the co-heating process. The formation of pigonite (Fe,Mg,-Ca)SiO_3 and johannsenite $CaMnSi_2O_6$ directly illuminates that the BG matrix reacted with the doping oxides. These reactions can change the original proportion of Fe_2O_3 and Mn_2O_3, and consequently reduce the production of $MnFe_2O_4$. In addition, the relative intensity of akermanite ($Ca_2MgSi_2O_7$) of MG was much lower than those of the mixture and BG. The doping oxides seem to inhibit the formation of akerminate. This may be attributed to the consumption of MgO to react with ferrite at high temperature. The XRD investigation in previous study revealed that spinel structure Mg ferrite started to form about 700°C and its fraction was increased with an increase of heat treatment temperature [34]. While $MgFe_2O_4$ was not observed in the XRD patterns of MG since this phase accounted for a small percent.

3.2 Magnetic property

The magnetic hysteresis loops of the mixture, the non-soaked MG and MG soaked in SBF for 30 days are shown in Fig. 2. The magnetic behaviour observed is similar to soft magnetic materials with narrow hysteresis loop and low coercivity. Under a magnetic field of 10,000 Oe, the saturation magnetization and the coercive force of the mixture are 26.2 emu/g and 50 Oe, respectively. While the non-soaked MG has a saturation magnetization of 6.4 emu/g and a coercive force of 198 Oe.

The doping of MnO_2 and Fe_2O_3 oxides leads to the magnetic behaviour of the glass ceramic. But when compared with the mixture, MG has a lower saturation magnetization value but a larger coercive force. The lower

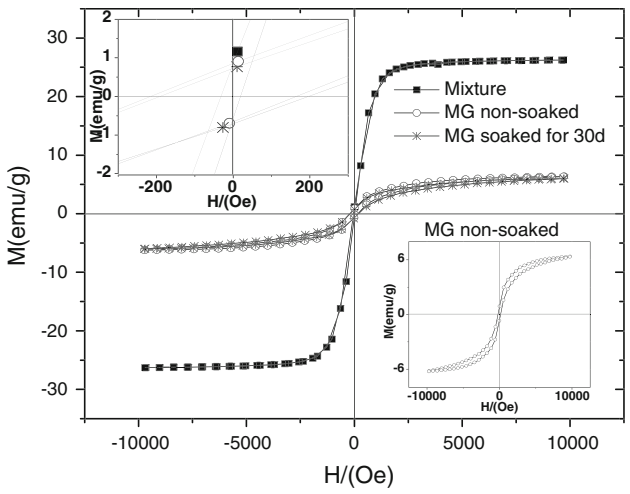

Fig. 2 Hysteresis loops of non-soaked MG, MG soaked in SBF for 30 days and the BG and ferrite mixture

saturation magnetization may be attributed to the reaction between the ferrite and BG matrix during the co-heating process. It was well known that P_2O_5 and SiO_2 can react with Fe_2O_3 easily at high temperature, forming non-magnetic phases, such as $Fe_2(SiO_3)_3$ and $FePO_4$ [35]. And Fe could also enter in the crystalline structure, forming solid solution, such as $CaSiO_3$·$FeSiO_3$ (ferroan wollastonite type) [36]. And the detection of pigonite (Fe,Mg,Ca)SiO_3 in MG reveals the reaction. Moreover, Mn could also react with the matrix at high temperature. Though the radius of Mn^{2+} (0.80 Å) is larger than that of Fe^{2+} (0.74 Å), the ionicity of Fe–O is weaker than that of Mn–O. Thus Mn^{2+} has almost the same opportunities to enter the silicate crystalline structure as Fe^{2+} [37]. And the formation of $CaMnSi_2O_6$ was detected in present study. The consumption of the magnetic elements Fe and Mn will inhibit the formation of magnetic phases, as a result, decrease the saturation magnetization. In addition, BG contains a lot of non-magnetic Si^{4+}, whose radius is smaller enough to enter the lattice of the spinel, could readily enter the spinel lattice and distort it [38]. Nevertheless the magnetic interaction can be effected in the distorted spinel lattice, and the saturation magnetization may be decreased.

Though the saturation magnetization of MG is lower than that of the ferrite and BG mixture, MG has a larger coercive force value. According to the literature, the coercive field is influenced in a significant way by the crystal dimensions [39]. Thus the average crystallite size of $MnFe_2O_4$ and Fe_3O_4 was calculated using Scherrer's formula [40]. The calculation results showed that the average crystallite size of $MnFe_2O_4$ and Fe_3O_4 was about 26 and 14 nm for MG, while 56 and 25 nm were obtained for the mixture. The smaller crystallite size of the magnetic phase in MG resulted in a larger coercive force. The as observed phenomena are similar to other researches [41].

Though MG showed lower saturation magnetization than the mixture, when compared with other magnetic bioactive glass–ceramics, a better magnetic behavior was obtained. The saturation magnetization and the coercive force of the specimen in present study were close to those of the glass–ceramic (having Fe_3O_4 as the magnetic phase) synthesized by Ruiz-Hernández et al. [42], however, less Fe_2O_3 was used in present work: Fe_2O_3 accounted for about 7 wt% in MG, while Fe_2O_3 accounted for about 22 wt% in their material. Furthermore, the bioactive glass–ceramics matrix in present study is similar to K. Sharma et al's research. The doping MnO_2 and Fe_2O_3 accounted for about 9.1 wt% in MG, the saturation magnetization of the material was 6.4 emu/g. While Fe_2O_3 accounted for about 15 wt% in Singh et al's material, but the saturation magnetization of the material was 3.75 emu/g [41].

Two reasons may be responsible for the better magnetic property of the material in present study. On the one hand,

the biphasic material process as Acros et al. used may be an important factor. As it was known, to obtain glass–ceramics which combine bioactivity and magnetic properties is not an easy task. The inclusion of Fe seems to diminish the bioactivity, and Fe is easily segregated, forming non magnetic precipitates while sintering. In order to solve the problem, Acros et al. synthesized a biphasic material containing a highly bioactive material (solgel-derived glass) and an other one with adequate magnetic properties (glass or glass–ceramic) [4, 7, 42]. In this way, over reactions between the magnetic elements and the matrix can be avoid and the bioactivity and magnetic property can be both improved. The biphasic material process used in present can prevent Fe and Mn reacting with the matrix too much, and better magnetic property can be obtained.

On the other hand, the doping oxides leaded to the formation of two magnetic phases $MnFe_2O_4$ and Fe_3O_4 in the sample. Both of the two phases have good magnetic property due to their spinel structure. In the spinel structure magnetic ions are distributed between two different lattice sites, tetrahedral (A) and octahedral (B) sites. It is well known that magnetic properties of ferrites depend on the distribution of cations at the different sites. We may write spinel structure ferrite MFe_2O_4 as $(M^{2+}_{\delta}Fe^{3+}_{1-\delta})[M^{2+}_{1-\delta}Fe^{3+}_{1+\delta}]O_4$, where M stands for divalent metal cation. Parentheses and square brackets denote cation sites of tetrahedral (A) and octahedral [B] coordination, respectively. δ represents the so-called degree of inversion (defined as the fraction of the (A) sites occupied by Fe^{3+} cations) [43]. In the spinel structure, the magnetic interaction between A and B sites is dominant and coupled in an antiparallel fashion. So, the molecular moment of MFe_2O_4, P_m may be expressed by the following equation:

$$P_m = [(1-\delta)m + (1+\delta)\times 5]_B - [\delta m + (1-\delta)\times 5]_A$$
$$\text{Bohr magneton} = (1-2\delta)m + 10\delta \text{ Bohr magneton} \quad (1)$$

where m is the magnetic moment of metal^{2+} ions, and Fe^{3+} ions have 5 Bohr magneton. The magnetic moment of Mn^{2+} is also 5 Bohr magneton. The magnetic moment of Fe^{2+} is 4 Bohr magneton. Thus theoretically P_m for $MnFe_2O_4$ is 5 Bohr magneton [33], and P_m for Fe_3O_4 is 4 Bohr magneton. We can roughly estimate the sample including both phases results in a larger saturation magnetization value.

After soaking in SBF for 30 days, the saturation magnetization and coercive force of MG decrease to 6.0 emu/g and 185 Oe, respectively. The decline of saturation magnetization could be explained by the formation of hydroxyapatite on MG as shown later, which would imply that the relative weight of the magnetic phase decreased.

Table 1 Saturation magnetization, coercive force and integrated loop area of non-soaked MG, MG soaked in SBF for 30 days and the BG and ferrite mixture

Magnetic and structural parameters	Sample		
	Mixture	MG non-soaked	MG soaked for 30 days
Saturation magnetization, Ms (emu/g)	26.2	6.4	6.0
Coercive field, Hc (Oe)	50	198	185
Interpolated hysteresis area ±10 kOe	3793.5	11121.5	11101.3

The decrease of the coercive force of the soaked could be explained by the stress relaxation of the crystalline phase [4].

An additional parameter of basic importance for the magnetic characterization of the materials is the area of the hysteresis loop. The hysteresis loop area of material was integrated and listed in Table 1. The integrated loop area was calculated for a maximum applied field of 10 kOe. It can be seen that the hysteresis loop area of MG is much larger than that of the mixture, which may be attributed to the higher coercive force of MG. Theoretically, under low magnetic field, the energy dissipated by the glass–ceramic samples can be estimated from the hysteresis loop area [6]. The as obtained results indicate that MG is capable of generating heat under a proper alternative magnetic field. Moreover, the saturation magnetization and the coercive force of the specimen in present study are close to those of the material synthesized by Ruiz-Hernández et al., and similar heat generating ability can be expected [42].

3.3 In vitro bioactivity

3.3.1 Effects of Ca^{2+} concentration and pH

The Ca^{2+} concentration and pH changes in SBF during the in vitro assay are shown in Fig. 3. For both of the materials, Ca^{2+} concentration presents the same trend, which is consistent with other researches [4, 17]. It can also be observed that both the average and peak Ca^{2+} concentration values of BG are much higher than those of MG, and it takes a longer time for MG to reach the maximum concentration. The doping of MnO_2 and Fe_2O_3 to BG decreases the calcium release ability of the material. Two main reasons may be responsible for this phenomenon. On the one hand, MG has less Ca^{2+} in the original composition. On the other hand, the reactions between the doping oxides and the BG matrix while sintering may not only consume some dissoluble Ca^{2+} but also inhibit Ca^{2+} release from the matrix. Previous study demonstrated that

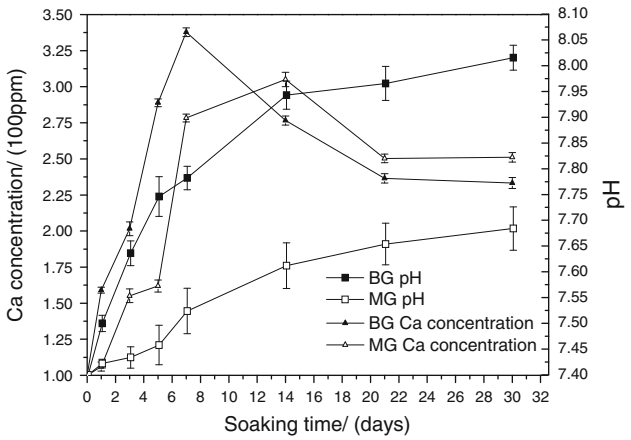

Fig. 3 Ca^{2+} concentration and pH value changes in SBF

the addition of Fe_2O_3 to glasses can decrease Ca^{2+} release ability due to the formation of Fe–O–P bonds that are more resistant to hydration than the P–O–P bonds [44].

Simultaneously with the Ca^{2+} release, a rapid increase of pH value occurred right after soaking. The release of Ca^{2+} and the pH increment agree with the mechanism proposed by Kokubo for the formation of an apatite-like layer on materials containing SiO_2–CaO in their composition [17, 45]. In such materials, an exchange of ions Ca^{2+} from material with H_3O^+ from the SBF is produced. The Ca^{2+} dissolved from the glass–ceramics increases the Ca^{2+} concentration in the SBF, and the consumption of H_3O^+ results in the increase of pH value. In present study, higher pH value is observed in accordance with higher Ca^{2+} concentration in BG.

3.3.2 *Morphological and spectra properties*

Figure 4 shows representative images of the surfaces of the MG and BG before and after soaking in SBF. Before soaking, samples surfaces were both made up by irregular particles of different sizes. But the surface of BG is observed to be denser, and it seems that MG has lower sintering ability. This phenomenon may be attribute to the sintering activity. The ferrite precursor was prepared by calcining oxides, and was not as active as sol–gel derived BG precursor. The doping ferrite may prevent the densification process.

After soaking in SBF for 7 days, globular precipitates coated the surface of BG. While no precipitates was observed on the surfaces of MG and the photo is not given. After soaking in SBF for 14 days, abundant globular aggregates were observed on the surface of MG, but the aggregates still did not form a continuous layer to cover the surface completely.

The XRD patterns of the detached deposits are shown in Fig. 5. Broad peaks are observed at 2θ about 26°, 29°, 32°, 34° and 50° for both of the samples, and hydroxyapatite phase [PDF #09-432] was identified. Wollastonite is observed in the pattern of MG. It because the coating was so little that the substrate contaminated the collected particles. The IR spectra of the deposits formed on the

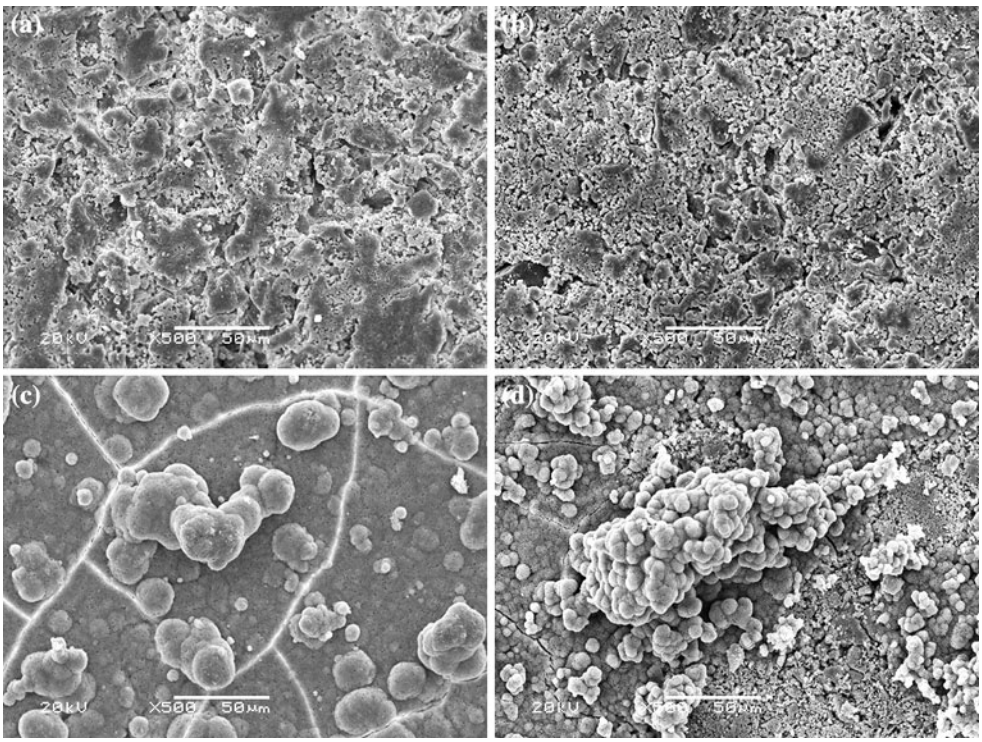

Fig. 4 Surface micrographs of: **a** non-soaked BG; **b** non-soaked MG; **c** BG soaked in SBF for 7 days, and **d** MG soaked in SBF for 14 days

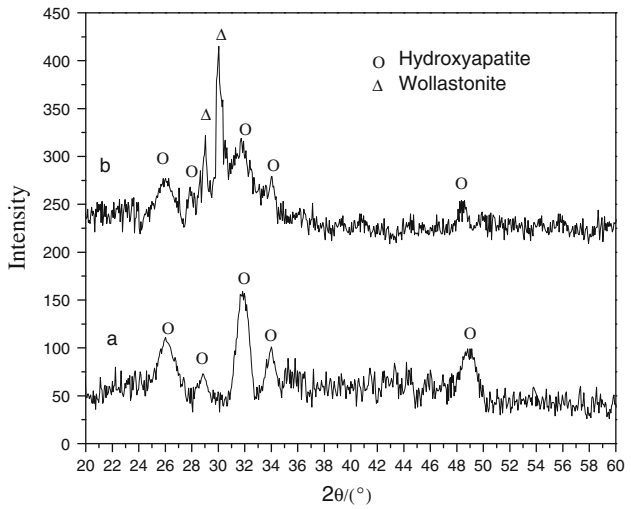

Fig. 5 XRD patterns of the detached precipitation formed on **a** BG soaked in SBF for 7 days and **b** MG soaked in SBF for 14 days

surfaces of samples are shown in Fig. 6. The as observed IR spectra is very similar to that of carbonate-containing hydroxyapatite formed on bioglasses in other researches [46]. Bands at 964 cm^{-1} is due to the P–O symmetric stretch, characteristic of hydroxyapatite [47]. Bands at 1,036, 964, 610 and 569 cm^{-1} are also attribute to the PO_4^{3-} IR absorption [48]. Bands between 1,400 and 1,500 cm^{-1} can be explained by the carbonate IR absorption. The band at 873 cm^{-1} is due to $HPO4^{2-}$ in hydroxyapatite [49], and also may be related to CO_3^{2-} vibrations [50]. The silicate IR absorption band around 1,100 cm^{-1} is observed in the spectrum for MG, which is in good agreement with the XRD results that wollastonite still existed [51]. Both the IR results and the XRD results are in accordance with the SEM results that the surface of

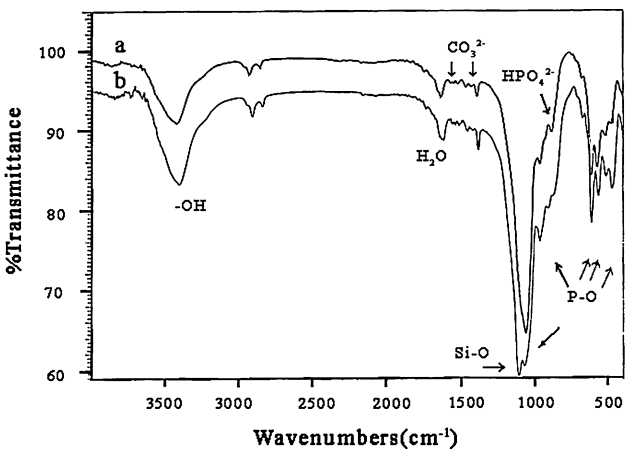

Fig. 6 FT-IR spectra of the detached precipitation formed on **a** BG soaked in SBF for 7 days and **b** MG soaked in SBF for 14 days

MG has not yet been covered by a complete aggregates layer.

In a comparison of the two materials, it takes a longer time for MG to form an apatite layer on the surface. This is in accord with the Ca^{2+} release ability of MG as discussed before. According to Kokubo's apatite formation mechanism, dissolution of Ca^{2+} to SBF causes the formation of hydrated silica, which provides favourable sites for apatite nucleation. Once the apatite nuclei are formed, they can grow spontaneously by consuming calcium and phosphate ions from the surrounding SBF. As SBF is super saturated with respect to the apatite, and moreover, the Ca^{2+} released from the matrix further increases the degree of supersaturation [45]. The samples that present a higher number of nucleation sites and that are exposed to fluid with higher Ca^{2+} concentration are able to develop an apatite coating more quickly.

Moreover, the morphology of the apatite coating appears to be different for the specimens under consideration. Whereas MG presents a non-continuous layer with uniform globular particles, BG shows this continuous layer together with some larger isolated aggregates. The non-continuous apatite layer formed on MG may be attributed to the inhomogeneous distribution of the sol–gel derived glass–ceramic on the surface [42]. The sol–gel glass–ceramic provides the sites for apatite nucleation. After that, a layer is formed on some zones of the material surface. The growth of this layer, however, is hindered by iron-containing grains. As a result, a non-continuous coating is not produced on the surface of MG. The larger isolated aggregates on BG may be due to heterogeneous nucleation and too long a period of exposition to SBF [52].

The presence of hydroxyapatite indicates that the materials are bioactive [17]. The doping of MnO_2 and Fe_2O_3 decreases the bioactivity of BG. When compared to the materials with similar magnetic properties in other research, the material in present work exhibits higher bioactivity. It took 21 days for the material in other research to form a non-continuous apatite layer on the surface, while only 14 days is needed in the present work [42]. The higher bioactivity of MG may be ascribed to the biophase process and less non-bioactive Fe_2O_3 contained in the material.

3.4 Cell affinity

In order to directly evaluate the interaction between materials and cells, SEM was carried out on the 7-day cell culture. Figure 7 shows the topical SEM micrographs of cells spreading on MG and BG during the co-culturing time. After 3 days of incubation, cells were observed on the surface of BG. The cells were still spherical in appearance. Therefore, it was assumed that cells were in

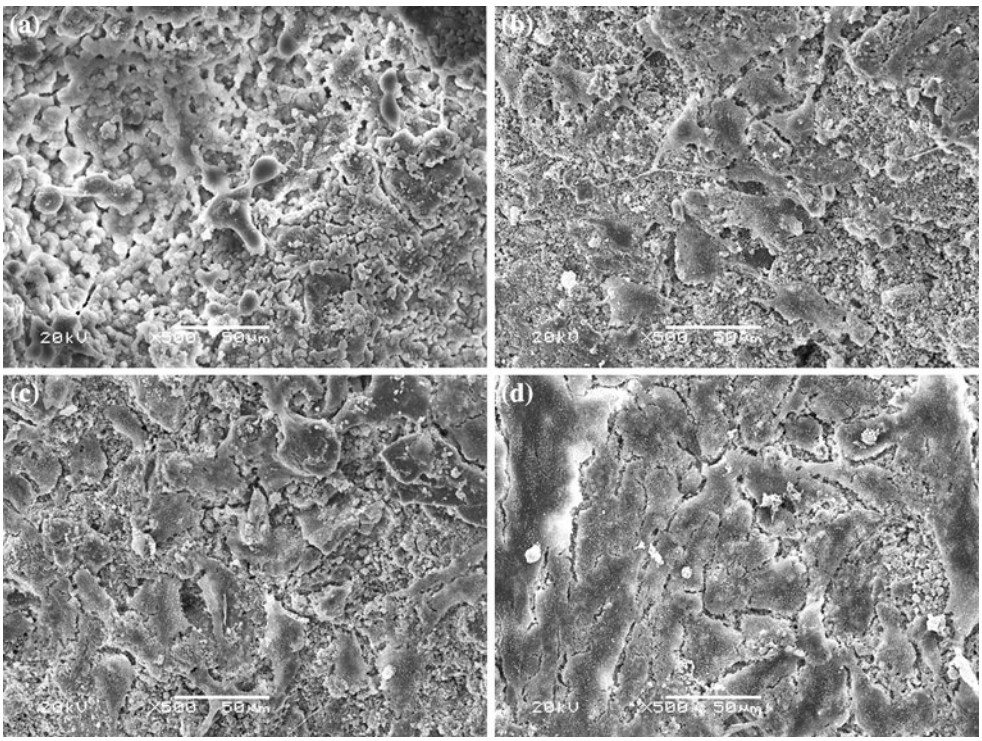

Fig. 7 SEM morphology of ROS17/2.8 cells after 3 days seeding on BG (**a**) and on MG (**b**); after 7 days seeding on BG (**c**) and on MG (**d**)

the early stage of cellular proliferation. Meanwhile cells were shown to be well attached and proliferated on the surfaces of MG. The cells stretched out lamellipodia and filopodia, anchoring themselves on the substrate firmly, and joined one to another. Some displayed star-like morphology, while others were fully spread, and mainly presented a flattened, osteoblast-like morphology [31]. After 7 days of incubation, many elongated cells are observed on the surface of BG. While cells on the surface of MG have dramatically reproduced and aggregated with each other, and almost completely spread on the sample forming a continuous layer. These results suggested that osteoblast-like cells can attach and proliferate well on the surface of MG, and the material has good cell affinity.

There are many factors that can influence the cell behaviour on materials, such as surface chemistry, surface roughness, surface energy and so on [53]. Normally, materials with better bioactivity has better cell affinity. Since the forming of apatite on the surface can greatly enhanced cell adhesion and proliferation [54]. For present study, though the bioactivity results showed that the addition of MnO_2 and Fe_2O_3 oxides decreased the bioactivity, the cell culturing experiments revealed that the doping oxides facilitated the cell adhesion and proliferation, and improved cell affinity of material. The doping Mn ion may play an important role on this phenomenon. Mn divalent cation is known to strongly influence the integrin avidity and the integrin affinity to ligands and—in consequence—cell adhesion to extracellular matrix proteins. In addition, the stimulating effect on the affinity maturation of $\alpha v\beta 1$-integrins is accompanied by focal adhesion organization and actin stress fiber formation, which is accompanied by enhanced cell migration [55]. Bigi et al. synthesized Mn-doped HA, and the biological tests demonstrated that the Mn-doped HA coatings favour osteoblasts proliferation, activation of their metabolism and differentiation [24]. Sima et.al prepared Mn-doped β-TCP, and their research showed that the 0.2 Mn-doped β-TCP showed higher potential for proliferation and better viability when tested in osteoprogenitor cell culture than did those with a lower Mn content [25]. Moreover, bioactive materials, and particularly bioactive glass–ceramics undergoing corrosion in aqueous solution, create a microenvironment that can influence cell response [53]. Hench pointed that the ions released from the glasses had effect on genes of cells [56]. The doping oxides changes the ion releasing ability of the material as shown by the SBF soaking test, which may be another important factor that influence the cell behaviour. Additional experiments must be performed for a better understanding of the relationship between the MnO_2 doping MG and the cells.

4 Conclusion

A novel magnetic bioactive glass–ceramic in the system $CaO–SiO_2–P_2O_5–MgO–CaF_2–MnO_2–Fe_2O_3$ was synthesized by doping MnO_2 and Fe_2O_3 to wollastonite–fluorapatite-containing glass–ceramics. And $MnFe_2O_4$ and Fe_3O_4 were detected to be the magnetic phases of the novel

material. Under a magnetic field of 10,000 Oe, the saturation magnetization and coercive force of the sample were 6.4 emu/g and 198 Oe, respectively. Though the doping of oxides decreased the bioactivity of the material, a lot of hydroxyapatite containing CO_3^{2-} were observed on the surface of MG after soaking in SBF for 14 days. The experiment of co-culturing ROS17/2.8 cells with material showed that the cells could successfully attach and well proliferate on the surface of MG, and MG showed better cell affinity than the original matrix. The material has the potential to be used as thermoseeds for hyperthermia.

Acknowledgment Financial support from the Research Fund for the Doctoral Program of Higher Education (20060610024) from Education Ministry of China and Doctoral Research Fund from Henan University of Science and Technology are gratefully acknowledged.

References

1. Hench LL, Splinter RJ, Allen WC, Greenlee TK. Bonding mechanisms at the interface of ceramic prosthetic materials. J Biomed Mater Res. 1971;2:117–41.
2. Ohura K, Ikenaga M, Nakamura T, Yamamuro T, Ebisawa Y, Kokubo T, et al. A heat-generating bioactive glass-ceramic for hyperthermia. J Appl Biomater. 1991;2:153–9.
3. Ebisawa Y, Miyaji F, Kokubo T, Ohura, Nakamura T. Bioactivity of ferrimagnetic glass-ceramics in the system FeO-Fe_2O_3-CaO-SiO_2. Biomaterials. 1997;18:1227–48.
4. Arcos D, Del Real RP, Vallet-Regì M. A novel bioactive and magnetic biphasic material. Biomaterials. 2002;23:2151–8.
5. Jiang Y, Jun O, Zhang Z, Qin Q-H. Preparation of magnetic and bioactive calcium zinc iron silicon oxide composite for hyperthermia treatment of bone cancer and repair of bone defects. J Mater Sci Mater Med. 2009;22:721–9.
6. Singh R, Srinivasan A, Kothiyal GP. Evaluation of CaO-SiO2–P2O5-Na2O-Fe2O3 bioglass-ceramics for hyperthermia application. J Mater Sci Mater Med. 2009;20:S147–51.
7. Arcos D, Del Real RP, Vallet-Regi M. Biphasic materials for bone grafting and hyperthermia treatment of cancer. J Bio Med Mater Res. 2003;65A:71–8.
8. Lung Fung T, Kwok Chuen W, Shekhar Madhukar K, Lin H, Tsun Cheung C, James Francis G. Bisphosphonates reduce local recurrence in extremity giant cell tumor of bone: a case–control study. Bone. 2008;42:68–73.
9. Lee YK, Lee SB, Kim YU, Kim KN, Choi SY, Lee KH, et al. Effect of ferrite thermoseeds on destruction of carcinoma cells under alternating magnetic field. J Mater Sci. 2003;38:4221–33.
10. Luderer AA, Borrelli NF, Panzarino JN, Mansfield GR, Hess DM, Brown JL, et al. Glass-ceramic-mediated, magnetic-field-induced localized hyperthermia: response of a murine mammary carcinoma. Radiat Res. 1983;94:190–8.
11. Ebisawa Y, Sugimoto Y, Hayashi T, Kokubo T, Ohura K, Yamamuro T. Crystallization of (FeO-Fe_2O_3)-CaO-SiO_2 glass and magnetic properties of their crystallized products. J Ceram Soc Jpn. 1991;99:7–13.
12. Bretcanu O, Spriano S, Verné E, Cöisson M, Tiberto P, Allia P. The influence on crystallised Fe_3O_4 on the magnetic properties of coprecipitation-derived ferrimagnetic glass-ceramics. Ata Biomater. 2005;1:421–9.
13. Singh R, Srinivasan A. Apatite-forming ability and magnetic properties of glass-ceramics containing zinc ferrite and calcium sodium phosphate phases. Mater Sci Eng C. 2010;30:1100–6.
14. Shah SA, Hashmi MU, Alam S, Shamim A. Magnetic and bioactivity evaluation of ferrimagnetic $ZnFe_2O_4$ containing glass ceramics for the hyperthermia treatment of cancer. J Magn Magn Mater. 2010;322:375–81.
15. Chi-Shiung H, Huy-Zu C, Hui-Ju H, Yung-Sheng C, Moo-Chin W. Crystallization kinetics and magnetic properties of iron oxide contained 25Li2O–8MnO2–20CaO-2P2O5–45SiO2 glasses. J Eur Ceram Soc. 2007;27:3171–6.
16. Tzu-Wei W, Hsi-Chin W, Wei-Ren W, Feng-Huei L, Pei-Jen L, Ming-Jium S, et al. The development of magnetic degradable DP-Bioglass for hyperthermia cancer therapy. J Biomed Mater Res. 2007;83A:828–37.
17. Kokubo T. A-W Glass-ceramics: processing and properties. In: Hench LL, Wilson J, editors. An introduction to bioceramics. Singapore: World Scientific; 1993. p. 75–88.
18. Sharma K, Dixit A, Jagannath SS, Bhattacharya S, Prajapat CL, Sharma PK, et al. Preparation and studies on surface modifications of calcium-silico-phosphate ferrimagnetic glass-ceramics in simulated body fluid. Mater Sci Eng C. 2009;29:2226–33.
19. Guangda L, Dali Z, Ming X, Weizhong Y, Qin L, Bin C, et al. Study on the surface bioactivity of novel magnetic A-W glass ceramic in vitro. Appl Surf Sci. 2008;25:559–61.
20. Guang Da L, Da Li Z, Yun L, Tao Hua P, Guo Sheng C, Qiu Dan Y. Synthesis and characterization of magnetic bioactive glass-ceramics containing Mg ferrite for hyperthermia. Mater Sci Eng C. 2010;30:148–53.
21. Culotta VC, Yang M, Hall MD. Manganese transport and trafficking: lessons learned from *Saccharomyces cerevisiae*. Eukaryot Cell. 2005;4:1159–65.
22. Paluszkiewicz C, Ślósarczyk A, Pijocha D, Sitarz M, Bućko M, Zima A, et al. Synthesis, structural properties and thermals stability of Mn-doped hydroxyapatite. J Mol Struct. 2010;976:301–9.
23. Mayer I, Gdalya S, Burghaus O, Reinen D, Cohen S. Crystal structure and EPR study of Mn-doped β-tricalcium phosphate. Mater Res Bull. 2008;43:447–52.
24. Bigi A, Bracci B, Cusinier F, Elkaim R, Fini M, Mayer I, et al. Human osteoblast response to pulsed laser deposited calcium phosphate coatings. Biomaterials. 2005;26:2381–9.
25. Sima F, Socol G, Axente E, Mihailescu IN, Zdrentu L, Petrescu SM, et al. Biocompatible and bioactive coatings of Mn^{2+}-doped β-tricalcium phosphate synthesized by pulsed laser deposition. Appl Surf Sci. 2007;254:1155–9.
26. Khalid MB. Study of dielectric and impedance properties of Mn ferrites. Phys B Condens Matter. 2011;406:382–7.
27. Khalid MB, Shalendra K, Chan GL, Alimuddin. Study of dielectric and ac impedance properties of Ti doped Mn ferrites. Curr Appl Phys. 2009;9:1397–406.
28. Jyotsnendu G, Pallab P, Vaibhav S, Hitesh C, Shreerang C, Rinti B, Dhirendra B. Synthesis and characterizations of water-based ferrofluids of substituted ferrites [Fe1-x BxFe2O4, B = Mn, Co(x = 0–1)] for biomedical applications. J Magn Magn Mater. 2008;320:724–30.
29. Ming X, Dan-Ge F, Guang-Da L, Wei-Zhong Y, Da-Li Z. Preparation of porous apatite-wollastonite bioactive glass ceramic (AW-GC) by dipping with polymer foams. J Inorg Chem. 2007;23:708–12.
30. Kokubo T, Takadama H. How useful is SBF in predicting in vivo bone bioactivity? Biomaterials. 2006;27:2907–15.
31. Skelton KL, Glenn JV, Clarke SA, Georgiou G, Valappil SP, Knowles JC, et al. Effect of ternary phosphate-based glass compositions on osteoblast and osteoblast-like proliferation, differentiation and death in vitro. Acta Biomater. 2007;3:56372.

32. Gallego D, Higuita N, Garcia F, Ferrell N, Hansford DJ. Bioactive coatings on Portland cement substrates: Surface precipitation of apatite-like crystals. Mater Sci Eng C. 2008;28:347–52.
33. Yao L, Jiuxing J, Jiupeng Z. X-ray diffractionand Mössbauer studies of phase transformation in manganese ferrite prepared by combustion synthesis method. Mater Chem Phys. 2004;87:91–5.
34. Jong-Gyu P, Man-Jong L, Sang-Hoon H. Reaction kinetics and formation mechanism of magnesium ferrites. Thermochim Acta. 2005;425:131–6.
35. Zhigang Z. Ferrite magnetic material. BeiJing: Science Press; 1981.
36. Ohashi Y, Finger LW. The role of octahedral cations in pyroxenoid crystal chemistry I. Bustamite, wollastonite, and the pectolite-schizo-lite-serandite series. Am Mineral. 1978;63:274–88.
37. Wager LR, Mitchell RL. The distribution of trace elements during strong fractionation of basic magma-a further study of the Skaergaard intrusion, East Greenland. Geochim Cosmochim Acta. 1951;1:129–208.
38. Shokrollahi H, Janghorban K. Influence of additives on the magnetic properties, microstructure and densification of Mn–Zn soft ferrites. Mater Sci Eng B. 2007;141:91–107.
39. Chikazumi S, Taketomi S, Ukita M, Mizukami M, Miyajima H, Seto-gawa M, et al. Physics of magnetic fluids. J Magn Magn Mater. 1987;65:24551.
40. Langford JI, Wilson AJC. Scherrer after sixty years: A survey and some new results in the determination of crystallite size. J Appl Cryst. 1978;11:102–13.
41. Singh R, Srinivasan A. Bioactivity of ferrimagnetic MgO-CaO-SiO2–P2O5-Fe2O3 glass-ceramics. Ceram Int. 2010;36:283–90.
42. Ruiz-Hernández E, Serrano MC, Arcos D, Vallet-Regí M. Glass–glass ceramic thermoseeds for hyperthermic treatment of bone tumors. J Biomed Mater Res. 2006;79A:533–43.
43. Šepelák V, Bergmann I, Menzel D, Feldhoff A, Heitjans P, Litterst FJ, et al. Magnetization enhancement in nanosized $MgFe_2O_4$ prepared by mechanosynthesis. J Magn Magn Mater. 2007;316:e764–7.
44. Abou Neel EA, Ahmed I, Blaker JJ, Bismarck A, Boccaccini AR, Lewis MP, et al. Effect of iron on the surface, degradation and ion release properties of phosphate-based glass micro-fibres. Acta Biomater. 2005;1:553–63.
45. Kokubo T, Matsushita T, Takadama H, Kizuki T. Development of bioactive materials based on surface chemistry. J Eur Ceram Soc. 2009;29:1267–74.
46. Xiaoxia Y, Xiaohui H, Chengzhong Y, Hexiang D, Yi W, Zhendong Z, et al. The in vitro bioactivity of mesoporous bioactive glasses. Biomaterials. 2006;27:3396–403.
47. Radin S, Ducheyne P, Rothman B, Conti A. The effect of in vitro modeling conditions on the surface reactions of bioactive glass. J Biomed Mater Res. 1997;37A:363–75.
48. Liang H, Wan YZ, He F, Huang Y, Xu JD, Li JM, et al. Bioactivity of Mg-ion-implanted zirconia and titanium. Appl Surf Sci. 2007;253:3326–33.
49. Xiaoyan L, Xudong L, Hongsong F, Xiantao W, Jian L, Xingdong Z. In situ synthesis of bone-like apatite/collagen nanocomposite at low temperature. Mater Lett. 2004;58:3569–72.
50. Inés B, Ingo H, Frank AM. Preparation of bioactive sodium titanate ceramics. J Eur Ceram Soc. 2007;27:4547–53.
51. Elbatal HA, Azooz MA, Khalil EMA, Monem AS, Hamdy YM. Characterization of some bioglass-ceramic. Mater Chem Phys. 2003;80:599–609.
52. Lopes PP, Leite Ferreira BJM, Almeida NAF, Fredel MC, Fernandes MHV, Correia RN. Preparation and study of in vitro bioactivity of PMMA-co-EHA composites filled with a $Ca_3(PO_4)_2$-SiO_2-MgO glass. Mater Sci Eng C. 2008;28:572–7.
53. Loty C, Forest N, Boulekbache H, Kokubo T, Sautier JM. Behavior of fetal rat chondrocytes cultured on a bioactive glass-ceramic. J Biomed Mater Res. 1997;37A:137–49.
54. Nieves O, Ana IM, Antonio JS, Javier T, Vallet-Regì M, Lizarbe MA. Bioactive sol-gel glasses with and without a hydroxycarbonate apatite layer as substrates for osteoblast cell adhesion and proliferation. Biomaterials. 2003;24:3383–93.
55. Lüthen F, Bulnheim U, Müller PD, Rychly J, Jesswein H, Nebe JG. Influence of manganese ions on cellular behavior of human osteoblasts in vitro. Biomol Eng. 2007;54:531–6.
56. Hench LL. Genetic design of bioactive glass. J Eur Ceram Soc. 2009;29:1257–65.